

Article

Vibration Control of a High-Rise Slender Structure with a Spring Pendulum Pounding Tuned Mass Damper

Qi Wang ^{1,2} , Hong-Nan Li ^{1,3} and Peng Zhang ^{4,*} 

¹ School of Civil Engineering, Shenyang Jianzhu University, Hunnan District, Shenyang 110168, China; wang-qi@stu.sjzu.edu.cn (Q.W.); hnli@dlut.edu.cn (H.-N.L.)

² Department of Road and Bridge Engineering, Liaoning Provincial College of Communications, Shenyang 110168, China

³ State Laboratory of Coastal and Offshore Engineering, Faculty of Infrastructure Engineering, Dalian University of Technology, Ganjingzi District, Dalian 116024, China

⁴ Institute of Road and Bridge Engineering, Dalian Maritime University, Dalian 116023, China

* Correspondence: peng.zhang47@dlmu.edu.cn

Abstract: High-rise structures are normally tall and slender with a large height-width ratio. Under the strong seismic action, such a structure may experience violent vibrations and large deformation. In this paper, a spring pendulum pounding tuned mass damper (SPPTMD) system is developed to reduce the seismic response of high-rise structures. This SPPTMD system consists of a barrel limiter with the built-in viscoelastic material and a spring pendulum (SP). This novel type of tuned mass damper (TMD) relies on the internal resonance feature of the spring pendulum and the collision between the added mass and barrel limiter to consume the energy of the main structure. Based on the Hertz-damper model, the motion equation of the structure-SPPTMD system is derived. Furthermore, a power transmission tower is selected to evaluate the vibration reduction performance of the SPPTMD system. Numerical results revealed that the SPPTMD system can effectively reduce structural vibrations; the reduction ratio is greater than that of the spring pendulum. Finally, the influence of the key parameters on the vibration control performance is conducted for future applications.

Keywords: high-rise structure; spring pendulum pounding tuned mass damper (SPPTMD) system; Hertz-damp model; equation of motion; parametric study



Citation: Wang, Q.; Li, H.-N.; Zhang, P. Vibration Control of a High-Rise Slender Structure with a Spring Pendulum Pounding Tuned Mass Damper. *Actuators* **2021**, *10*, 44. <https://doi.org/10.3390/act10030044>

Academic Editors: Emiliano Pereira González, Paul Reynolds and Sumeet S. Aphale

Received: 4 February 2021
Accepted: 24 February 2021
Published: 28 February 2021

Publisher's Note: MDPI stays neutral with regard to jurisdictional claims in published maps and institutional affiliations.



Copyright: © 2021 by the authors. Licensee MDPI, Basel, Switzerland. This article is an open access article distributed under the terms and conditions of the Creative Commons Attribution (CC BY) license (<https://creativecommons.org/licenses/by/4.0/>).

1. Introduction

High-rise infrastructures such as skyscrapers, wind turbines, radio or television towers and power transmission towers are featured by its low damping and high vulnerability under seismic hazards. Damages or collapse of high-rise structures have been extensively reported in post-earthquake investigations. For example, in the Kobe earthquake of 1995 and the Wenchuan earthquake of 2008, more than a dozen transmission towers were damaged [1]. Similarly, strong winds can also cause the collapse of large wind turbine towers [2] and antenna towers [3]. Mitigation of the undesired vibrations of these structures can effectively improve the structural safety and reliability.

In engineering, controlling the vibration of high-rise structures is an effective practice for reducing the dynamic responses of these structures. A variety of damping devices and damping algorithms has been proposed, including eddy current damper [4–7], electromagnetic damper [8], LQR controller [9], magnetorheological damper [10], tuned liquid column damper [11], particle damper [12,13], etc. Among these damping devices, the tuned mass damper (TMD) is widely accepted due to its simple structure, low cost and convenient installation. When the primary structure is forced into motion, the TMD can generate an inertial force to reduce the structural vibration. In recent years, scholars have conducted considerable research on the TMD and proposed many new type TMD devices, such as the annular TMD [14], pendulum TMD [15,16], frictional TMD [17], viscoelastic TMD [18,19].

Weber et al. [20,21] designed a semi-active tuned mass damper with magnetorheological damper, which can control structures that vibrate at different frequencies. Scholars used piezoelectric ceramics to change the curvature of the bending beam [22] and the prestress imposed on the steel plate [23] to change the stiffness of the damper, thereby achieving effective vibration control of the structure within a certain frequency range. A TMD based on a piezoelectric transducer has been proposed. The advantage of this damper is that it has adaptive resonance frequency and damping, and low energy consumption [24]. To improve the vibration resistance of the dampers, scholars also introduced shape memory alloys [25–28] into the TMD. Tian et al. proposed a type of TMD composed of nonlinear shape memory alloys [29]. Salvi et al. [30] performed a parametric study of the TMD and achieved optimal design. Chen et al. [31] studied an eddy current tuned mass damper (ECTMD). Elias et al. [32] reduced the wind vibration of chimneys by TMD. In order to further improve the performance of TMDs [33] and avoid performance degradation due to changes in their system parameters [34,35], scholars have also investigated multi-TMDs [36,37].

The passive control methods are the most widely applied to the field of civil engineering [38,39]. Since the TMD is a linear vibration absorber, its frequency band of vibration suppression is relatively narrow compared with the nonlinear vibration absorbers [40]. Therefore, previous researchers have introduced nonlinear components, such as the cubic spring [41], pounding components [42–44], internal resonance [45] or nonlinear short wire ropes [46] to the classical TMD device, so as to widen its frequency band.

The pounding tuned mass damper (PTMD), which consists of a mass block and a limiter, is a typical nonlinear damper. The PTMD utilizes the inertial force of the added mass and the collision between the added mass and limiter to consume the kinetic energy of the structure and then achieve vibration control effect. Previous studies have shown that the PTMD is superior to traditional TMD in vibration control for the high-rise slender structures, and it has the advantages of a wider vibration suppression frequency band [47,48] and better robustness [49]. Therefore, the PTMD has been widely applied to control vibrations in various structures, such as power transmission towers [50], frame structures [51], traffic signal structures [52], bridges [53–55], pipeline structures [56–58], voided biaxial concrete slab [59] and stay cable [60]. Additionally, scholars have verified their effectiveness through experiments [61,62] and numerical simulations. Collete [63] et al. confirmed the oscillation suppression effectiveness of a tuned absorber combined with an impact damper. Wang et al. [64] performed numerical methods to simulate the energy consumption process of absorber. Li et al. [49] examined the robustness and seismic performance of the PTMD using numerical methods and experimental studies. Lin et al. [65] analyzed the vibration reduction effect of the PTMD and multiple PTMDs (MPTMDs) on the basis of a modified pounding force model [66]. Furthermore, in order to control the wind-induced response of the transmission tower, Fu et al. [67] devised a new pounding spacer damper (PSD). More recently, a bidirectional PTMD [68] and a damper with zero distance from the tuned mass to the collision boundary [69] have been presented. The combination of a PTMD and a shape memory alloy are used by Ghasemi et al. [70] to reduce the vibration of offshore jacket platforms.

The spring pendulum (SP) composing of a mass block hanged by a spring is another typical nonlinear damper [71,72]. Motion of the mass block can be decomposed into two vibration modes: (1) the radial vibration mode, in which the mass block vibrates along the radius direction; (2) the swing mode, in which the mass block swings in the tangential direction, as a classical pendulum. If a specific relation between the spring stiffness and pendulum length is satisfied, an internal resonance phenomenon will occur, in which vibration energy will be transferred between the two modes, i.e., the internal resonance phenomenon [73]. A previous study has demonstrated that the SP can effectively reduce structural vibration [45] and is superior to the traditional TMD in vibration absorption. Nevertheless, the additional damping element is not included in the previous SP damper. Consequently, its energy dissipation capacity is still insufficient and introducing an additional damping may further improve the vibration control effectiveness. Collision between

the added mass of the SP and some limiter can be a beneficial method of introducing additional energy dissipation. Therefore, this paper incorporates the collision into the SP and proposes a new type damper, namely the spring pendulum pounding tuned mass damper (SPPTMD). The SPPTMD is composed of a connecting plate, a mass, spring and a limiter built-in viscoelastic material. Compared with the traditional TMD, energy absorbing ability of the SPPTMD was enhanced by the internal resonance phenomenon. Compared with the SP damper, the energy dissipation of the SPPTMD was enhanced by the collision.

The remaining parts of this article are arranged as follows. Section 2 introduces the configurations and mechanism of the SPPTMD system. Section 3 deduces the equations of motion for the SPPTMD system and the structure-SPPTMD system based on the Hertz-damp model. Section 4 verifies the effectiveness of the SPPTMD system by considering a transmission tower model excited by three real earthquake waves. Section 5 discusses the oscillation mitigation effectiveness of the SPPTMD due to variations in pounding stiffness, mass ratio, damping ratio and gap, which were undertaken analytically. Finally, a summary is provided in Section 6 to close this paper.

2. Mechanism of the SPPTMD

The SPPTMD is a novel damping device developed on the basis of suspended mass pendulum (SMP) and SP. In order to clearly demonstrate the mechanism of the proposed SPPTMD, schematics of the SMP, the SP and the SPPTMD are all illustrated and compared in this section.

2.1. Mechanism of the SMP

As is illustrated in Figure 1, the suspended mass pendulum (SMP) is basically a suspended mass block connected to the structure to be controlled by a cable. The length of the cable is carefully designed to adjust the frequency of the SMP to match the frequency of the structure, in order to obtain optimal damping effectiveness. The length of the cycloid can be calculated by the following Equation [16]:

$$l = g / (2\pi f)^2, \quad (1)$$

where $g = 9.8 \text{ m/s}^2$ is gravitational acceleration; f is the frequency of the primary structure.

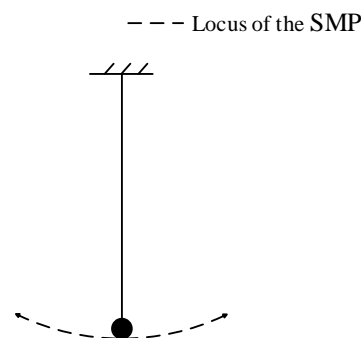


Figure 1. Locus of the suspended mass pendulum.

2.2. Mathematical Model of the SP

The SP can be regarded as a modified SMP, which replaces the suspending cable with a linear spring. In previous studies [45,71,72], the motion equation of the SP has been derived to analyze its behavior. Suppose the original length and the stiffness of the spring are l_{ori} and k_s , respectively. When the mass is subjected to gravity, length of the spring will be stretched to l_0 (as shown in Figure 2):

$$l_{ori} = l_0 - \frac{m_d g}{k_s} \quad (2)$$

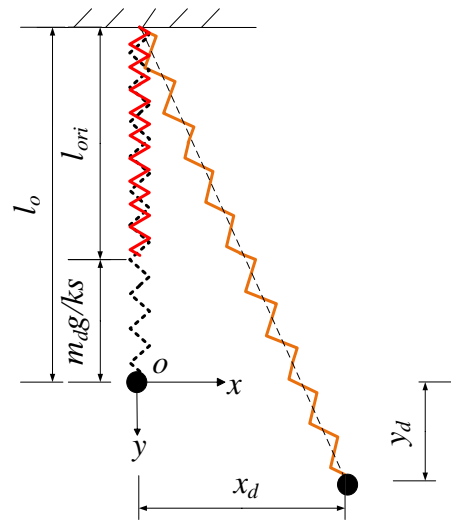


Figure 2. Schematic of the spring pendulum (SP).

Suppose this position is the origin point O and establishing a coordinate (Figure 2), the motion equation is as follows:

$$\begin{cases} \ddot{x}_d + \frac{k_s x_d}{m_d} \left(1 - \frac{l_{ori}}{\sqrt{x_d^2 + (y_d + l_0)^2}}\right) = 0 \\ \ddot{y}_d + \frac{k_s}{m_d} (y_d + l_0) \left(1 - \frac{l_{ori}}{\sqrt{x_d^2 + (y_d + l_0)^2}}\right) - g = 0 \end{cases} \quad (3)$$

where x_d and y_d denote the displacement of the SP in the horizontal and vertical direction; k_s is the stiffness of the spring; m_d is the mass of the mass block; l_{ori} is the original length of the spring; l_0 denotes the length of the spring under the load of gravity; $g = 9.8 \text{ m/s}^2$ is gravitational acceleration.

At any moment, the spring will add a nonlinear restoring force to the mass block of the SP in both x and y directions:

$$\begin{cases} f_x = k_s x_d \left(1 - \frac{l_{ori}}{\sqrt{x_d^2 + (y_d + l_0)^2}}\right) \\ f_y = k_s y_d \left(1 - \frac{l_{ori}}{\sqrt{x_d^2 + (y_d + l_0)^2}}\right) - m_d g \end{cases} \quad (4)$$

Since the mass block is suspended by a spring in the SP, it has two coupled vibration modes: the radial vibration mode and the swing vibration mode. The radial vibration mode allow the mass block to move in the radius direction, while in the swing mode, the mass block moves like a pendulum (Figure 3). The circular frequency of the radial mode is determined by the mass and stiffness of the spring:

$$\omega_s = \sqrt{\frac{k_s}{m}} \quad (5)$$

in which ω_s is the circular frequencies of the radial vibration mode; k_s is the stiffness of the spring; m is the mass of the mass block. In the swing mode, the mass block vibrates like a pendulum; the circular frequency of this mode can be determined by:

$$\omega_p = \sqrt{\frac{g}{l_0}} \quad (6)$$

where ω_p is the circular frequencies of the swing mode; l_0 is the length of the spring under the load of gravity.

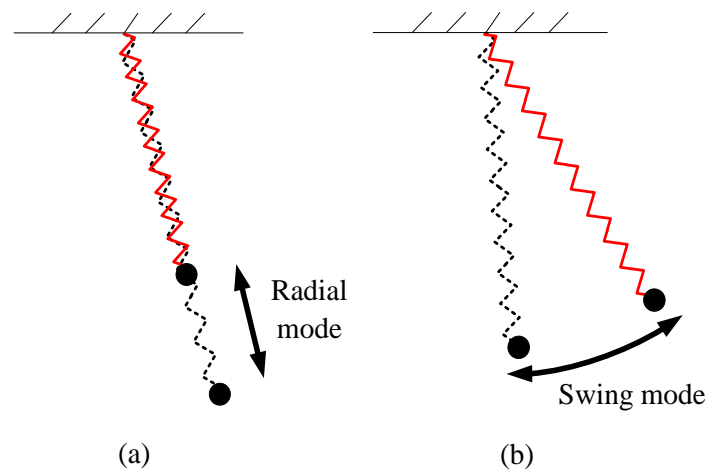


Figure 3. Vibration modes of the SP. (a) Radial mode; (b) Swing mode.

In previous studies, it is found that if the ratio of ω_s over ω_p is near 2, the two vibration modes are strongly coupled, and energy can be transferred between these two modes. This phenomenon is named as internal resonance and

$$\lambda = \frac{\omega_s}{\omega_p} = 2 \quad (7)$$

is named as internal resonance condition. In order to verify the motion equation of the SP, a numerical model is established in MATLAB and the trajectory of an SP subjected to an initial displacement is calculated and illustrated in Figure 4. It can be seen that the trajectory of the SP is very consistent with the conclusion in the literature [71].

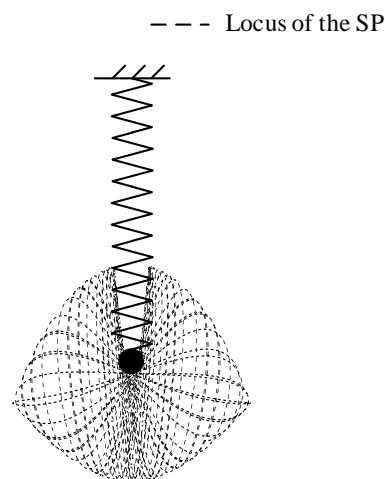


Figure 4. Locus of the SP.

It should also be noted that the suspended mass pendulum can be regarded as a special SP, whose spring stiffness is very large; thus, the radial vibration mode is often neglected. Compared with the SMP, the SP has two strongly coupled vibration modes, which effectively increases its energy absorption ability.

2.3. Mechanism of the SPPTMD

Though previous studies also demonstrate that its energy absorption ability of the SP is larger compared to the suspended mass pendulum, because the SP has an additional radial vibration mode [45], the energy dissipation capacity of the SP is still insufficient. Therefore, this paper incorporates the collision into the SP. As seen in Figure 5, the SPPTMD

system consists of a connection plate, a mass block, a spring and a limiter with the built-in viscoelastic material. Among these components, the connection plate is employed to connect the SPPTMD system to the main structure, while the spring pendulum and the limiter are used to absorb the vibration energy; additionally, the viscoelastic material is applied to reduce the noise generated when the mass collides with the limiter, to avoid local damage of the limiter and to increase the energy consumption during collision. The vibration suppression principle of the SPPTMD system is as follows: (i) when the vibration of the primary structure is small, the mass of the SPPTMD absorbs the kinetic energy of the primary structure as a typical SP; (ii) when the vibration of the primary structure exceeds a certain level, the added mass collides on the limiter and dissipate the absorbed kinetic energy.

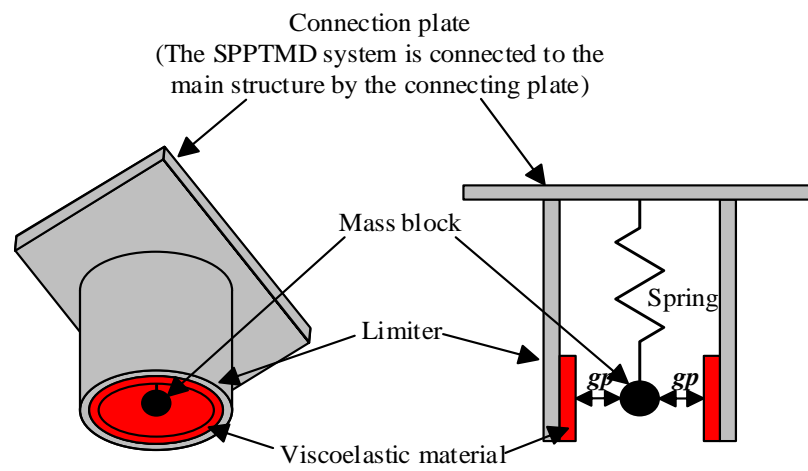


Figure 5. Spring pendulum pounding tuned mass damper (SPPTMD) system designed for controlling the vibration of a structure.

3. Numerical Model of the Structure-SPPTMD System

Figure 6 demonstrates an n -degree-of-freedom (DOF) structure equipped with an SPPTMD at the i th floor. It can be seen from Figure 7 that the is subjected to two forces, i.e., the restoring force (F_s) generated by the relative motion and the impact force (F_c) when the SPPTMD collides on the boundary.

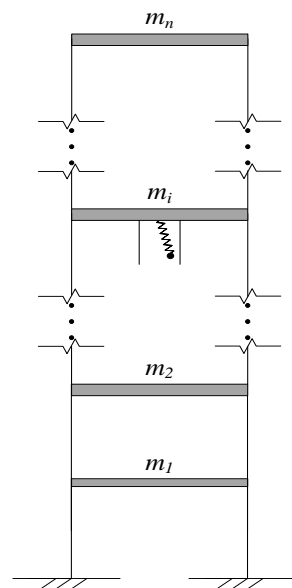


Figure 6. Schematic of the structure-SPPTMD system.

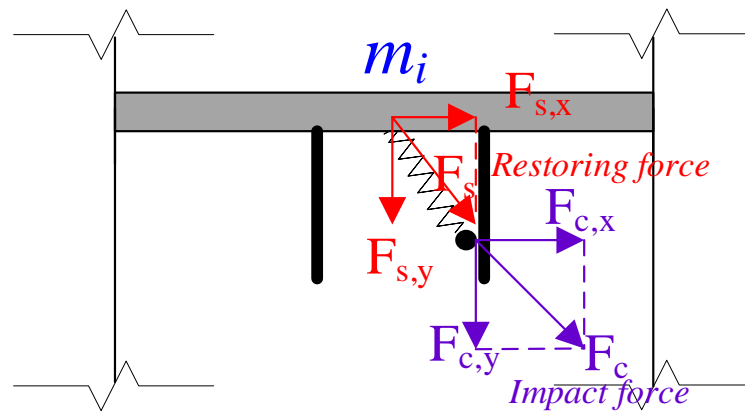


Figure 7. Controlling forces imposed on the i th degree of freedom (DOF).

Suppose the displacement of the i th DOF is x_i , and the displacement of the SPPTMD is x_d and y_d in the horizontal and vertical direction. Then the relative displacement between the damper and the i th floor is

$$x_r = x_d - x_i \tag{8}$$

$$y_r = y_d \tag{9}$$

Similar to Equation (4), the restoring force generated by the relative motion is:

$$\begin{cases} F_{s,x} = k_s x_r \left(1 - \frac{l_{ori}}{\sqrt{x_r^2 + (y_r + l_o)^2}}\right) \\ F_{s,y} = k_s y_r \left(1 - \frac{l_{ori}}{\sqrt{x_r^2 + (y_r + l_o)^2}}\right) - m_d g \end{cases} \tag{10}$$

Suppose the gap between the SPPTMD and the boundary is g_p , then the relative deformation of the elastic material attached to the surface of the boundary can be expressed as follows:

$$\delta = \begin{cases} x_r - g_p & \text{if impacts the right boundary} \\ -x_r + g_p & \text{if impacts the left boundary} \end{cases} \tag{11}$$

and the speed of the deformation is:

$$\dot{\delta} = \dot{x}_r \tag{12}$$

The impact force generated by the collision can be attained based on the Hertz contact model [50]:

$$F_c = \begin{cases} \beta \delta^{1.5} + c \dot{\delta} & \text{if } \dot{\delta} > 0 \\ \beta \delta^{1.5} & \text{if } \dot{\delta} < 0 \end{cases} \tag{13}$$

in which β is the pounding stiffness and c is the impact damping. c can be calculated by

$$c = 2\zeta \sqrt{\beta \frac{m_d m_i}{m_d + m_i}} \tag{14}$$

where ζ is the impact damping ratio; m_d and m_i are the mass of the SPPTMD and the i th floor. ζ can be attained by:

$$\zeta = \frac{9\sqrt{5}}{2} \frac{1 - e^2}{e[e(9\pi - 16) + 16]} \tag{15}$$

Here, $e = \sqrt{\frac{h^*}{h}}$ is the restitution coefficient which can be determined by dropping a sphere on the surface of the elastic material and measure the initial height, h , and bounced height, h^* . In this paper, $\beta = 17,000 \text{ N/m}^{3/2}$ and $e = 0.25$ is obtained from previous experimental studies [50].

It should be noted that the mass block of the SPPTMD can impact either on the left side or the right side of the two boundaries. Therefore, F_{dir} is defined to indicate the direction of the pounding force:

$$F_{dir} = \begin{cases} 1 & x_d - x_i > g_p & \text{pounding on the right side} \\ -1 & x_d - x_i < -g_p & \text{pounding on the left side} \\ 0 & \text{others} & \text{not pounding} \end{cases} \quad (16)$$

Based on Equations (8)–(16), the equations of motion for an n -degree-of-freedom structure equipped with an SPPTMD attached to the i th degree of freedom can be derived as follows:

$$\begin{cases} \mathbf{M}_s \ddot{\mathbf{x}}(t) + \mathbf{C}_s \dot{\mathbf{x}}(t) + \mathbf{K}_s \mathbf{x}(t) = -\mathbf{M}_s \mathbf{I} \ddot{x}_g(t) + \mathbf{L} F_{s,x}(t) + F_{dir} \mathbf{L} F_{c,x}(t) \\ m_d \ddot{x}_d(t) = -F_{s,x}(t) - F_{dir} F_{c,x}(t) \\ m_d \ddot{y}_d(t) = m_d g - F_{s,y}(t) - F_{c,y}(t) \end{cases} \quad (17)$$

where \mathbf{M}_s , \mathbf{C}_s and \mathbf{K}_s are the mass, damping and stiffness matrices of the undamped structure, respectively; $\ddot{\mathbf{x}}(t)$, $\dot{\mathbf{x}}(t)$ and $\mathbf{x}(t)$ are the acceleration, velocity and displacement vectors, respectively; \mathbf{I} is a column vector of ones; \ddot{x}_g is the ground acceleration; and \mathbf{L} denotes the location of the SPPTMD; F_s is the nonlinear force generated by the spring of the SPTMD; F_{dir} denotes the direction of the impact; F_c is the nonlinear pounding force; m_d is the mass of the mass block; x_d and y_d denote the displacement of the SPPTMD in the horizontal and vertical direction; $F_{s,y}$ and $F_{c,y}$ are the restoring force and the pounding force, respectively, of the spring pendulum in the y direction.

In Equation (17), suppose the SPPTMD is attached to the i th degree of freedom of the primary structure, then the location vector \mathbf{L} is as follows:

$$\mathbf{L} = \left(0, 0, \dots, \underbrace{1}_{\text{the } i\text{th element equals one}}, 0, \dots, 0 \right)^T \quad (18)$$

Equation (17) is modeled in a Simulink environment of MATLAB and solved by the ODE45, which is an embedded solver based on Runge–Kutta Method. The time step size is variable, with the maximum step size set to 0.02 s. All other parameters are set to the default values of the software.

4. Case Study

To demonstrate the vibration damping performance of the SPPTMD, a numerical analysis is performed based on a 53.9 m high power transmission tower [45], which is a typical high-rise structure. As shown in Figure 8, the transmission tower is simplified by 15 DOFs, and has a mass of 19,621 kg and a natural frequency of 1.87 Hz. The layout of the SPPTMD on the transmission tower is illustrated in Figure 9.

In this paper, three recorded ground motions are chosen according to Chinese Code for designing transmission tower structures [74], to verify the effectiveness of the proposed SPPTMD, with their peak acceleration adjusted to 400 cm/s². The detailed information of the selected seismic records is shown in Table 1. Afterward, the damping performance of an SMP, an SP and an SPPTMD with the same mass ratio are compared. The following parameters are assumed for the numerical study: the mass ratio is 2%, the damping ratio is 2%, $\beta = 17,000 \text{ N/m}^{3/2}$, $g_p = 0.05 \text{ m}$. The seismic responses of the tower under the various earthquake waves are shown in Figures 10–12.

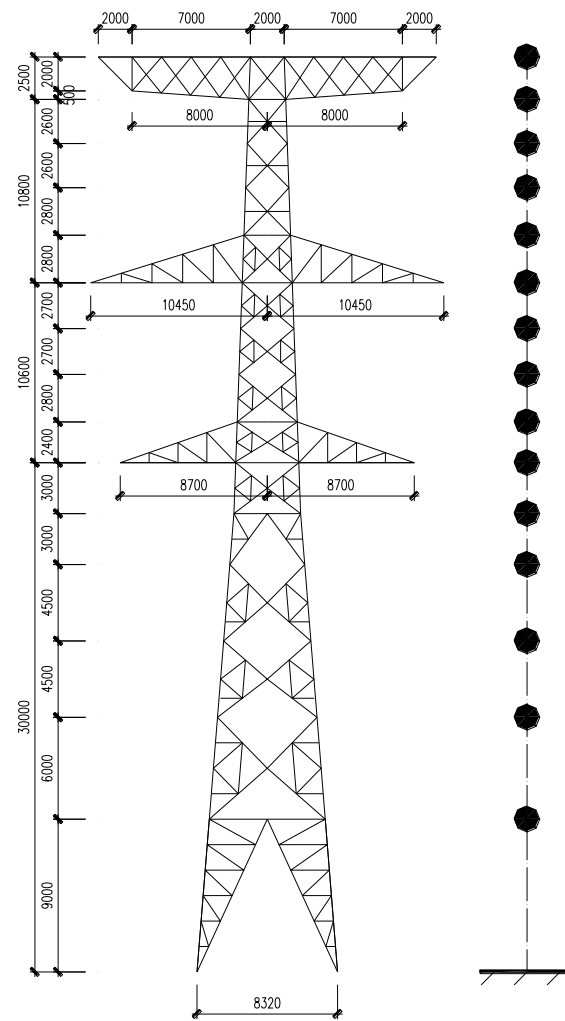


Figure 8. Schematic of the transmission tower.

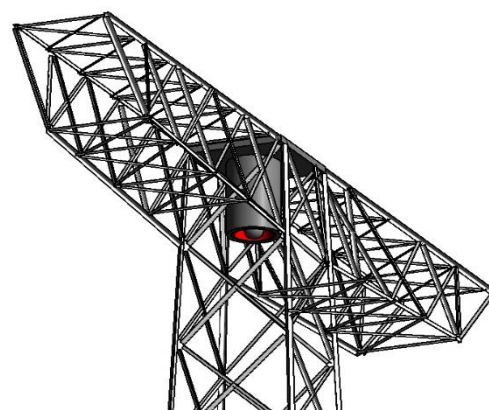
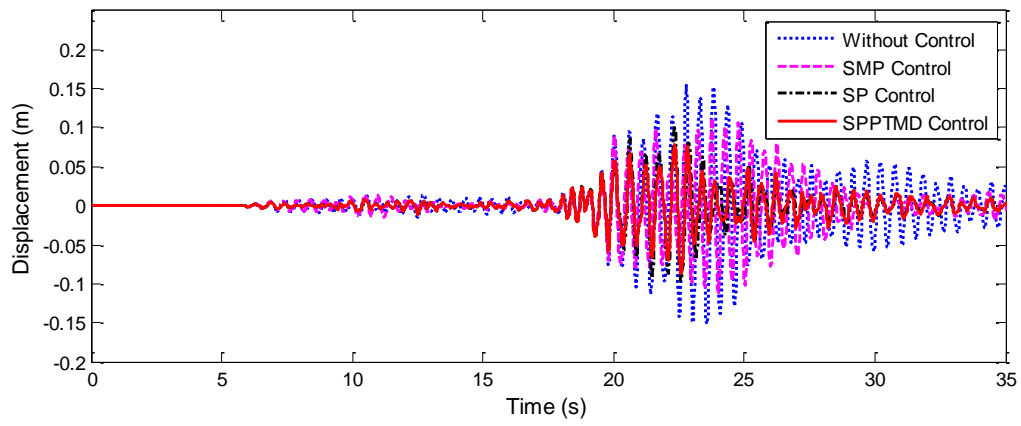


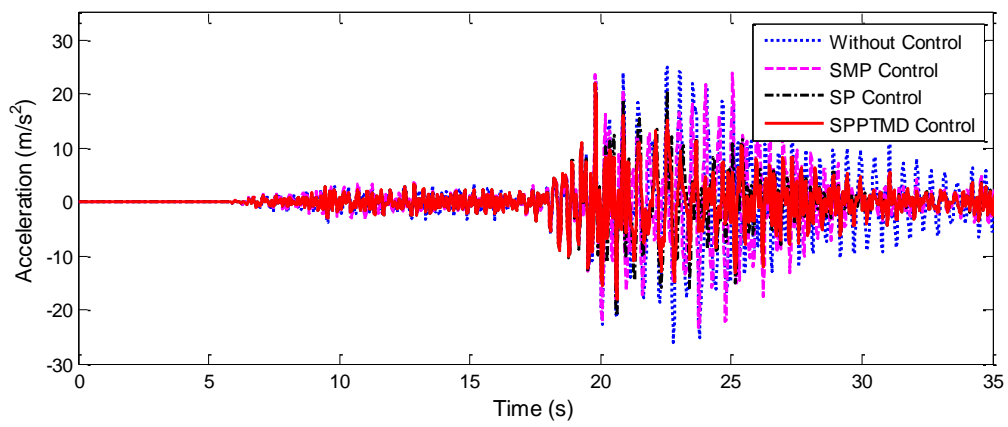
Figure 9. Layout of the SPPTMD on the transmission tower.

Table 1. Seismic records.

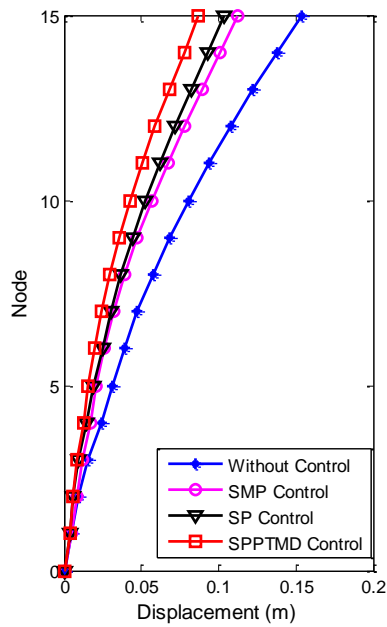
ID	Earthquake	Event Date	Magnitude	Station
EQ1	Kobe	16 January 1995	6.9	Oka
EQ2	Northridge	17 January 1994	6.6	Villa Park-Scrrano Avc
EQ3	Kobe	16 January 1995	6.9	Takatori



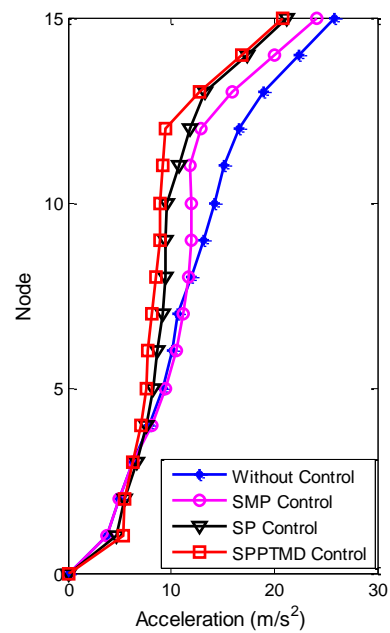
(a)



(b)



(c)



(d)

Figure 10. Seismic response of the tower top under EQ1: (a) displacement; (b) acceleration; (c) envelope of displacement; and (d) envelope of acceleration.

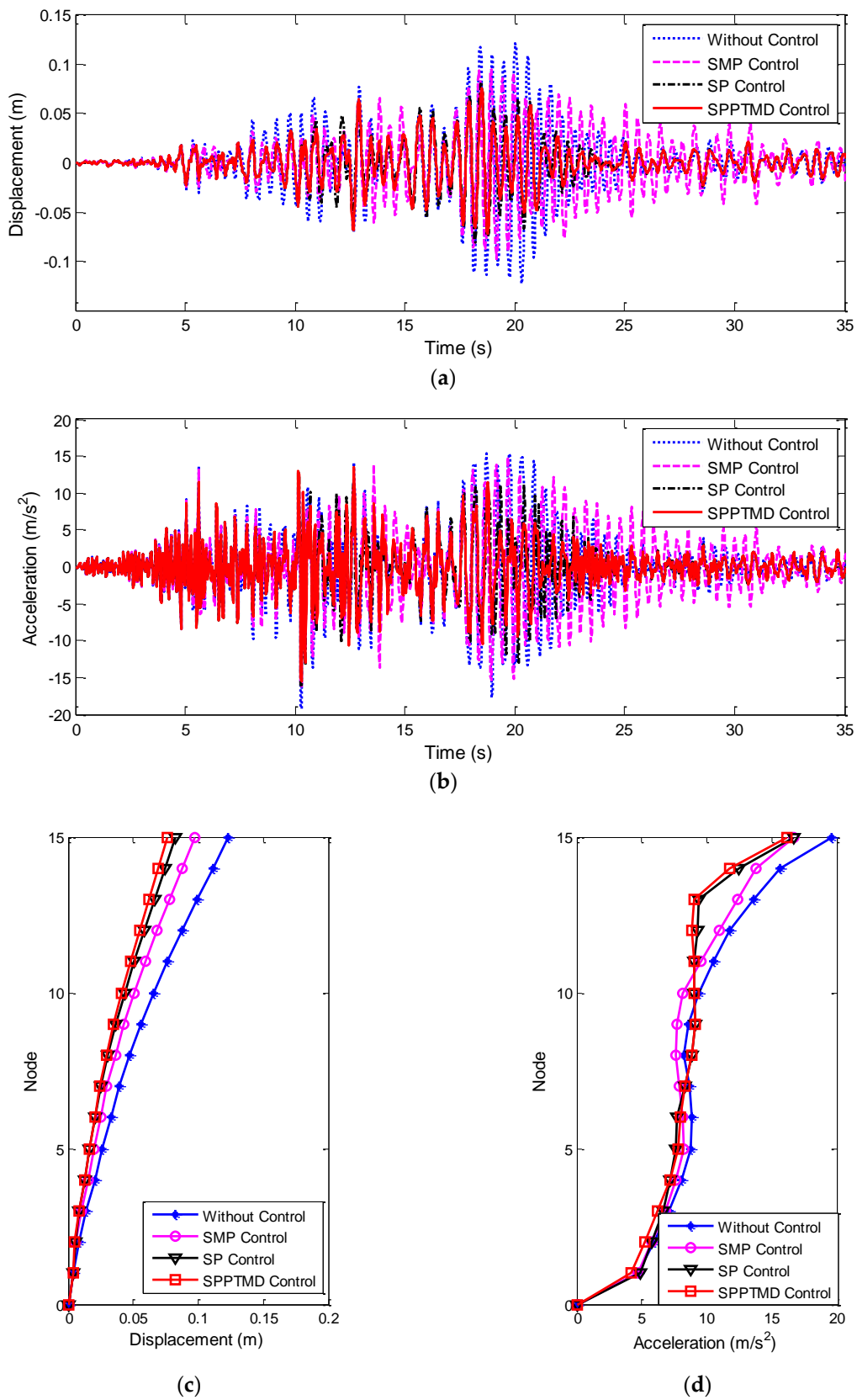


Figure 11. Seismic response of the tower top under EQ2: (a) displacement; (b) acceleration; (c) envelope of displacement; and (d) envelope of acceleration.

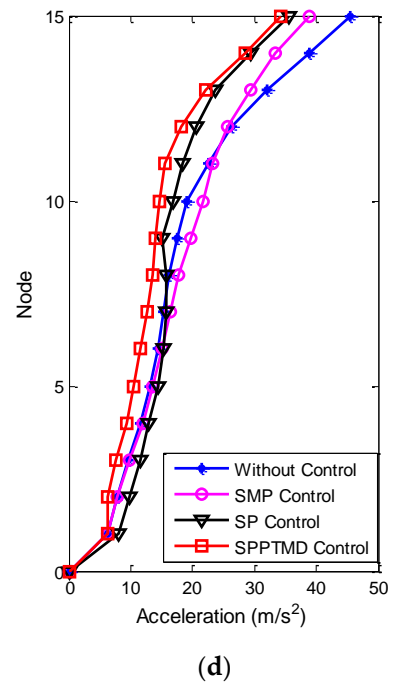
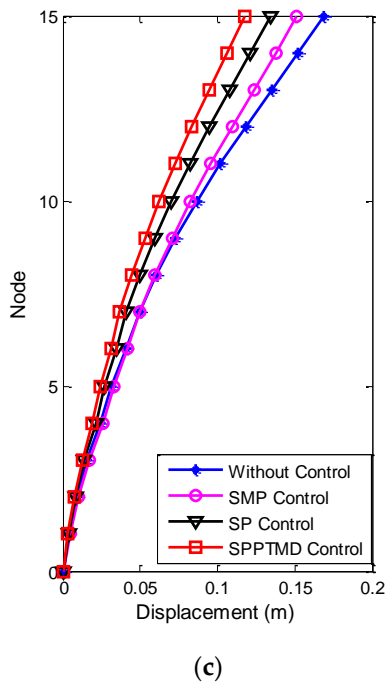
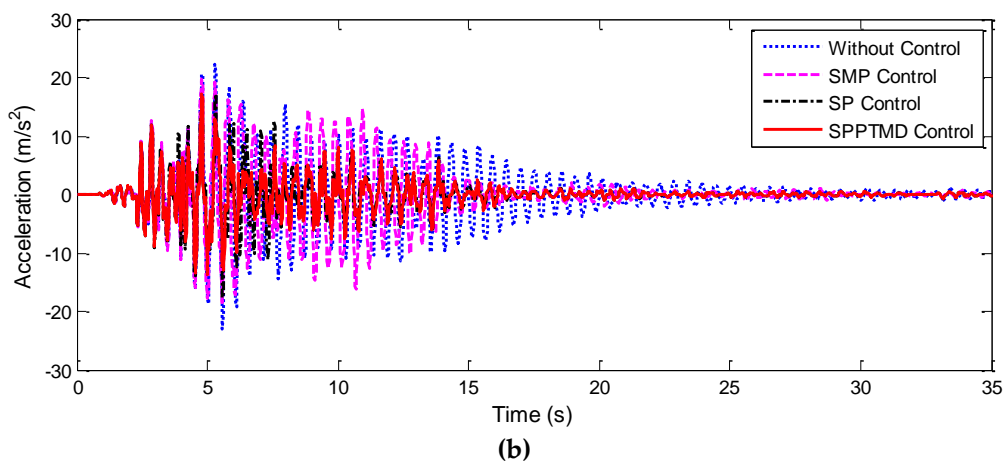
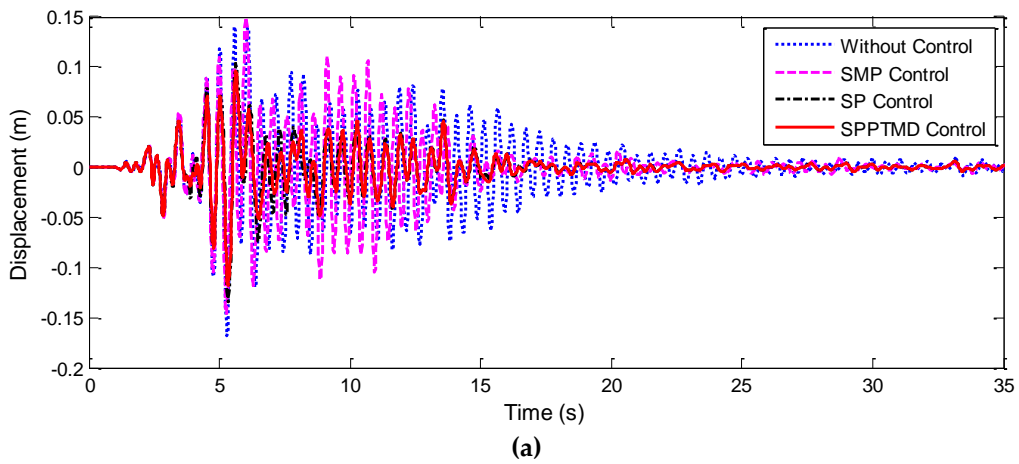


Figure 12. Seismic response of the tower top under EQ3: (a) displacement; (b) acceleration; (c) envelope of displacement; and (d) envelope of acceleration.

To quantify the damping performance of the SPPTMD, the vibration reduction ratio is defined as follows:

$$\eta_d = \frac{(D_0 - D_1)}{D_0} \times 100\% \quad (19)$$

$$\eta_a = \frac{(A_0 - A_1)}{A_0} \times 100\% \quad (20)$$

where D_1 and D_0 represent the displacements of the tower with and without control, respectively; and A_1 and A_0 are the acceleration responses of the tower with and without control, respectively. Table 2 lists the peak value and the root mean square (RMS) value of the seismic response of the tower.

Table 2. Vibration reduction ratios of the transmission tower.

Earthquake	Damper	η_d (%)		η_a (%)	
		Peak (%)	RMS (%)	Peak (%)	RMS (%)
EQ1	With SPPTMD	43.3	55.0	15.4	41.9
	With SP	32.9	48.4	15.3	34.7
	With SMP	26.7	24.7	7.7	14.8
EQ2	With SPPTMD	37.3	30.8	18.0	32.5
	With SP	29.8	27.4	15.3	29.9
	With SMP	21.3	7.0	15.7	0.8
EQ3	With SPPTMD	32.0	49.7	34.9	49.5
	With SP	20.9	42.4	25.4	41.6
	With SMP	10.4	5.2	14.0	0.02
Average	With SPPTMD	37.5	45.2	22.8	41.3
	With SP	27.9	39.4	18.7	35.4
	With SMP	19.5	12.3	12.5	5.2

It can be seen from Figures 10–12 that the vibration reduction ratio of SP and SPPTMD are slightly better compared with SMP. Especially in terms of the vibration reduction ratios of the displacement, SP and SPPTMD increased by more than 6% and 16%, respectively. Figure 10 indicates that the SP and the SPPTMD can both reduce the vibration caused by earthquakes on transmission tower. However, the displacement and acceleration reduction ratios of the SPPTMD are larger than that of the SP. Compared to the SP, the vibration reduction ratios of the displacement and acceleration are increased by 10.4% and 0.1%, respectively, with the SPPTMD. The damping performance of the SPPTMD is better than the SP because the pounding between the added mass and the delimiter provided additional energy dissipation approach. Generally, the ability of the damper to reduce displacement is better than the acceleration. In terms of the RMS value of the displacement and acceleration, more effective suppression is achieved by the SPPTMD, with vibration reduction ratios of 55% and 41.9%, whereas those of the SP are only 48.4% and 34.7%, respectively.

Figures 11 and 12 show the better results. Under EQ2, the reduction ratios of the displacement, acceleration, RMS of the displacement and RMS of the acceleration are 37.3%, 18%, 30.8% and 32.5%, respectively, when the SPPTMD is applied, which are greater than those of the SP, i.e., 29.8%, 15.3%, 27.4% and 29.9%. Similarly, under EQ3, compared to the SP, the displacement and acceleration reduction ratios of the transmission tower can be increased by the SPPTMD from 20.9% to 32.0% and from 25.4% to 34.9%, respectively. With regard to the RMS value of the displacement and acceleration, greater reduction ratios are also observed with the SPPTMD, increasing from 42.4% to 49.7% and from 41.6% to 49.5%, respectively. Obviously, numerical results indicate that the SPPTMD has a slightly improved vibration control performance under various earthquakes.

5. Parametric Study

Although the vibration reduction performance of the proposed SPPTMD has been verified numerically in the above Section 4, the influences of this damper's key parameters are not discussed. In this section, the pounding stiffness, the mass ratio, the gap between the added mass and the limiter and the damping ratio of the primary structure are selected as the key design parameters of the SP; their influence on the vibration reduction ratio are discussed to achieve further understanding of the damper and provide some suggestion for optimal design. Unless mentioned otherwise, all parameters have the same values as in Section 4.

5.1. Pounding Stiffness

The pounding stiffness of the viscoelastic materials is an important parameter in the numerical study. Its value may influence the vibration control effect of the proposed SPPTMD. Therefore, in this section, three values ($\beta = 5000 \text{ N/m}^{3/2}$, $\beta = 17,000 \text{ N/m}^{3/2}$ and $\beta = 50,000 \text{ N/m}^{3/2}$) were used to study its influence and the vibration reduction ratio η_d is employed to interoperate the vibration control performance. When the pounding stiffness β is set to $5000 \text{ N/m}^{1.5}$, $17,000 \text{ N/m}^{1.5}$ and $50,000 \text{ N/m}^{1.5}$, the reduction ratios are 40.3%, 43.3% and 44.4%. This indicates that the vibration control effectiveness can be upgraded with the increasement of pounding stiffness. However, this improvement is very slightly. The time history of the tower with the three level of β are also illustrated in Figure 13. It can be seen that the curves are very close, which also indicate that the pounding stiffness has little influence on the damping effect of the SPPTMD. This conclusion is similar to that of the PTMD, as in previously announced in the literature [50].

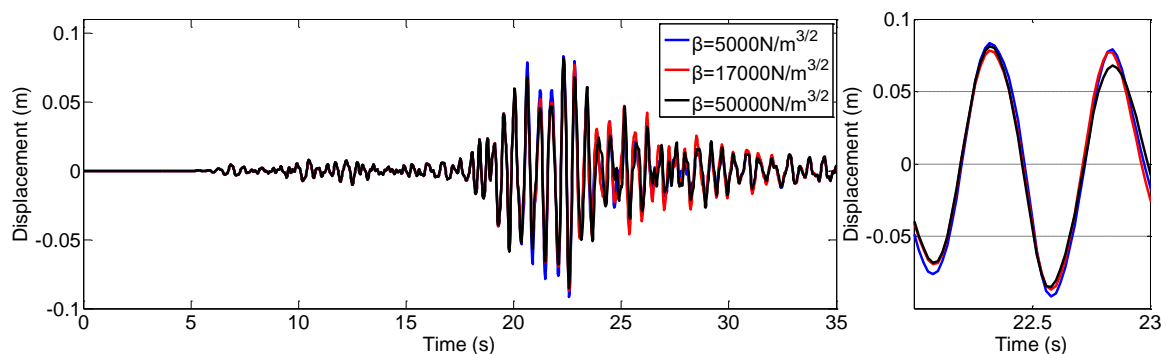


Figure 13. Displacement at the top of the tower with different pounding stiffness values.

5.2. Mass Ratio

To study the influence of the mass ratio on the damping effect, the vibration reduction ratio of the transmission tower controlled by applying the SPPTMD with mass ratios from 1.5% to 3% was calculated. As plotted in Figure 14, the larger the mass ratio is, the better the damping effect of the SPPTMD is. However, considering the influence of the economic factor, it is suggested that the mass ratio of the TMD be 2% [75]. It can be seen from Figure 14, when the mass ratio is 2%, the vibration reduction ratio is 43.3%.

5.3. Gap

Gap is an important factor, because the SPPTMD relies on the collision between the mass block with the limiter to consume the kinetic energy of the tower. The vibration reduction ratio curves of the SPPTMD with different mass ratios and gaps are shown in Figure 14. As a result that the swing of the mass block decreases increasing mass ratio, to ensure that the mass block can collide with the viscoelastic material, there must be different optimal gaps at different mass ratios. The numerical results indicate that the optimal gap decreases from 8 cm to 4 cm when the mass ratio increases from 1.5% to 3%. Moreover, the optimal gap has a range for every case. In addition, if the gap is too large, no collision

will occur. Take the case of a mass ratio of 2% as an example, the gap can be selected from 4 cm to 10 cm. When the gap is larger than 16 cm, the mass block does not collide with the viscoelastic material; in this case, the SPPTMD equates with the SP.

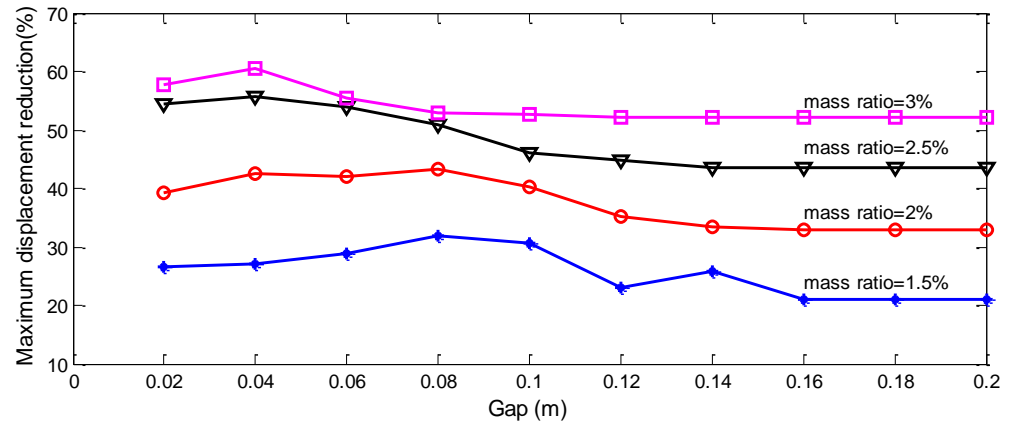


Figure 14. Displacement vibration reduction ratio of the tower with different mass ratios.

5.4. Damping Ratio of the Structure

The vibration reduction ratios of the tower with different damping ratios are given in Table 3. Obviously, the vibration reduction ratios of the displacement and acceleration of the SPPTMD are better than those for the SP. The SPPTMD can reduce the top displacement and acceleration by 51.7% and 30.4% for a primary structure with damping ratio of 0.5%. If the damping ratio of the primary structure reaches 5%, the vibration reduction ratios of the displacement and acceleration are only 32.4% and 6.8%, respectively. All these results indicated that the SPPTMD has a better vibration control performance on structures with low damping.

Table 3. Vibration reduction ratios of the tower with different damping ratios.

Damping Ratio (%)	Damper	η_d (%)		η_a (%)	
		Peak (%)	RMS (%)	Peak (%)	RMS (%)
0.5	With SPPTMD control	51.7	75.4	30.4	63.3
	With SP control	42.0	71.6	27.8	59.2
2	With SPPTMD control	43.3	55.0	15.4	41.9
	With SP control	32.9	48.4	15.3	34.7
5	With SPPTMD control	32.4	40.3	6.8	24.4
	With SP control	27.3	34.3	7.8	18.8

6. Conclusions

In this paper, a novel damping device with the name of spring pendulum pounding tuned mass damper is proposed for vibration control of high-rise structures. The SPPTMD consists of a mass block hanged by a spring (the SP part) and a barrel delimiter to restrain the motion of the mass. Governing equation of an m.d.o.f. structure damped by an SPPTMD is derived. A realistic power transmission tower is selected as the high-rise structure to be controlled, to validate the damping ability of the proposed SPTMD. Furthermore, a parametric study was also conducted to investigate the influence of pounding stiffness, mass ratio, gap and damping ratio on the damping effect. Based on these numerous numerical results, the following findings can be concluded:

1. Vibration control performance of the proposed SPPTMD is slightly improved compared with the SP and SMP. The maximum displacements of the tower are reduced by SMP, SP and SPPTMD by 19.5%, 27.9% and 37.5%, respectively. For the RMS value

of the displacement, reduction ratios are 12.3%, 39.4% and 45.2%, also demonstrating the superiority of the SPPTMD.

2. Vibration reduction ratio of the relative displacement is larger than that of the acceleration. The reduction ratio of the peak value and RMS value of the displacement is 37.5% and 45.2%, respectively. However, reduction ratio of the peak acceleration and RMS acceleration is only 22.8% and 41.3%.
3. In the parametric study, the pounding stiffness has little influence on the damping effect. When the pounding stiffness is increased by 10 times, the displacement vibration reduction ratio at the maximum pounding stiffness is only 6.9% higher than that of the minimum pounding stiffness.
4. Larger vibration reduction ratio can be achieved by increasing the mass ratio of the SPPTMD. This is similar to the classical TMD or PTMD.
5. The damping effectiveness is influenced by the gap. The optimal gap is determined by the mass ratio. When the mass ratio increases from 1.5% to 3%, the maximum displacement reduction ratio increases from 31.88% to 60.57% and the optimal gap decreases from 8 cm to 4 cm.
6. Damping ratio of the primary structure also influences the vibration reduction ratio of the SPPTMD. As the structural damping ratio increased from 0.5% to 5%, the reduction ratio of displacement drops from 51.7% to 32.4%.

Author Contributions: All authors discussed and agreed upon the idea, and made scientific contributions. Conceptualization, P.Z. and H.-N.L.; methodology, Q.W.; software, Q.W.; validation, Q.W., H.-N.L. and P.Z.; formal analysis, Q.W.; investigation, P.Z.; resources, H.-N.L.; data curation, P.Z.; writing—Original draft preparation, Q.W.; writing—Review and editing, P.Z.; visualization, P.Z.; supervision, H.-N.L.; project administration, H.-N.L.; funding acquisition, H.-N.L. All authors have read and agreed to the published version of the manuscript.

Funding: The authors would like to sincerely thank the financial supports from the State Key Program of National Natural Science Foundation of China (51738007 and 51808092).

Conflicts of Interest: The authors declare no conflict of interest.

References

1. Shinozuka, M. The Hanshin-Awaji earthquake of January 17, 1995 performance of lifelines. In *Technical Report NCEER*; US National Center for Earthquake Engineering Research (NCEER): Buffalo, NY, USA, 1995; Volume 95.
2. Chou, J.-S.; Tu, W.-T. Failure analysis and risk management of a collapsed large wind turbine tower. *Eng. Fail. Anal.* **2011**, *18*, 295–313. [[CrossRef](#)]
3. Repetto, M.P.; Solari, G. Wind-induced fatigue collapse of real slender structures. *Eng. Struct.* **2010**, *32*, 3888–3898. [[CrossRef](#)]
4. Abdo, T.M.; Huzayyin, A.A.; Abdallah, A.A.; Adly, A.A. Characteristics and Analysis of an Eddy Current Shock Absorber Damper Using Finite Element Analysis. *Actuators* **2019**, *8*, 77. [[CrossRef](#)]
5. Ao, W.K.; Reynolds, P. Evaluation of eddy current damper for vibration control of a frame structure. *J. Phys. Commun.* **2019**, *3*, 055013. [[CrossRef](#)]
6. Ao, W.K.; Reynolds, P. Analytical and experimental study of eddy current damper for vibration suppression in a footbridge structure. In *Dynamics of Civil Structures*; Springer: Berlin/Heidelberg, Germany, 2017; Volume 2, pp. 131–138.
7. Ao, W.K.; Reynolds, P. Optimal Analysis, Design and Testing of an Electromagnetic Damper with Resonantshunt Circuit for Vibration Control of a Civil Structure. In Proceedings of the 23rd International Congress of Sound and Vibration, Athens, Greece, 10–14 July 2016.
8. Ao, W.K.; Reynolds, P. Analysis of H_∞ and H_2 Optimal Design Scheme for an Electromagnetic Damper with Shunt Resonant Circuit. In *Shock & Vibration, Aircraft/Aerospace, and Energy Harvesting*; Springer: Berlin/Heidelberg, Germany, 2015; Volume 9, pp. 201–212.
9. Nyawako, D.S.; Reynolds, P. LQR controller for an in-service floor. In *Dynamics of Civil Structures*; Springer: Berlin/Heidelberg, Germany, 2011; Volume 4, pp. 227–237.
10. Puma-Araujo, S.D.; Olvera-Trejo, D.; Martínez-Romero, O.; Urbikain, G.; Elías-Zúñiga, A.; Lacalle, L.N.L.D. Semi-Active Magnetorheological Damper Device for Chatter Mitigation during Milling of Thin-Floor Components. *Appl. Sci.* **2020**, *10*, 5313. [[CrossRef](#)]
11. Kim, J.; Park, C.-S.; Min, K.-W. Fast vision-based wave height measurement for dynamic characterization of tuned liquid column dampers. *Measurement* **2016**, *89*, 189–196. [[CrossRef](#)]

12. Gnanasambandham, C.; Fleissner, F.; Eberhard, P. Enhancing the dissipative properties of particle dampers using rigid obstacle-grids. *J. Sound Vib.* **2020**, *484*, 115522. [[CrossRef](#)]
13. Lu, Z.; Liao, Y.; Huang, Z. Stochastic response control of particle dampers under random seismic excitation. *J. Sound Vib.* **2020**, *481*, 115439. [[CrossRef](#)]
14. Tabatabai, H.; Mehrabi, A.B. TMD-Damped Stay Cable and Method and TMD. Google Patents US6292967B1, 25 September 2001.
15. Battista, R.C.; Rodrigues, R.S.; Pfeil, M.S.; Aerodynamics, I. Dynamic behavior and stability of transmission line towers under wind forces. *J. Wind Eng.* **2003**, *91*, 1051–1067. [[CrossRef](#)]
16. He, Y.; Lou, W.; Sun, B. Wind-induced vibration control of long span transmission tower with suspended mass pendulums. *J. Zhejiang Univ. Eng. Sci.* **2005**, *39*, 1891.
17. Li, G.; Li, H.-N. Experimental study and application of metallic yielding–friction damper. *J. Earthq. Tsunami* **2013**, *7*, 1350012. [[CrossRef](#)]
18. Batou, A.; Adhikari, S. Optimal parameters of viscoelastic tuned-mass dampers. *J. Sound Vib.* **2019**, *445*, 17–28. [[CrossRef](#)]
19. Xu, Z.-S. Structure design, mathematical modeling and dynamical performance tests of a new viscoelastic elastomer damper. *Measurement* **2020**, 108820. [[CrossRef](#)]
20. Weber, F.; Boston, C.; Maślanka, M. An adaptive tuned mass damper based on the emulation of positive and negative stiffness with an MR damper. *Smart Mater. Struct.* **2010**, *20*, 015012. [[CrossRef](#)]
21. Weber, F.; Maślanka, M. Frequency and damping adaptation of a TMD with controlled MR damper. *Smart Mater. Struct.* **2012**, *21*, 055011. [[CrossRef](#)]
22. Bonello, P.; Brennan, M.J.; Elliott, S.J. Vibration control using an adaptive tuned vibration absorber with a variable curvature stiffness element. *Smart Mater. Struct.* **2005**, *14*, 1055. [[CrossRef](#)]
23. Gsell, D.; Feltrin, G.; Motavalli, M. Adaptive tuned mass damper based on pre-stressable leaf-springs. *J. Intell. Mater. Syst. Struct.* **2007**, *18*, 845–851. [[CrossRef](#)]
24. Heuss, O.; Salloum, R.; Mayer, D.; Melz, T. Tuning of a vibration absorber with shunted piezoelectric transducers. *Arch. Appl. Mech.* **2016**, *86*, 1715–1732. [[CrossRef](#)]
25. Rustighi, E.; Brennan, M.; Mace, B. A shape memory alloy adaptive tuned vibration absorber: Design and implementation. *Smart Mater. Struct.* **2004**, *14*, 19. [[CrossRef](#)]
26. Berardengo, M.; Della Porta, G.E.; Manzoni, S.; Vanali, M. A multi-modal adaptive tuned mass damper based on shape memory alloys. *J. Intell. Mater. Syst. Struct.* **2019**, *30*, 536–555. [[CrossRef](#)]
27. Savi, M.A.; De Paula, A.S.; Lagoudas, D.C. Numerical investigation of an adaptive vibration absorber using shape memory alloys. *J. Intell. Mater. Syst. Struct.* **2011**, *22*, 67–80. [[CrossRef](#)]
28. Tiwari, N.D.; Gogoi, A.; Hazra, B.; Wang, Q. A shape memory alloy-tuned mass damper inerter system for passive control of linked-SDOF structural systems under seismic excitation. *J. Sound Vib.* **2021**, *494*, 115893. [[CrossRef](#)]
29. Tian, L.; Zhou, M.; Qiu, C.; Pan, H.; Rong, K. Seismic response control of transmission tower-line system using SMA-based TMD. *Struct. Eng. Mech.* **2020**, *74*, 129–143.
30. Salvi, J.; Rizzi, E. Optimum tuning of Tuned Mass Dampers for frame structures under earthquake excitation. *Struct. Control Health Monit.* **2015**, *22*, 707–725. [[CrossRef](#)]
31. Chen, J.; Lu, G.; Li, Y.; Wang, T.; Wang, W.; Song, G. Experimental study on robustness of an eddy current-tuned mass damper. *Appl. Sci.* **2017**, *7*, 895. [[CrossRef](#)]
32. Elias, S.; Matsagar, V.; Datta, T.K. Along-wind response control of chimneys with distributed multiple tuned mass dampers. *Struct. Control Health Monit.* **2019**, *26*, e2275. [[CrossRef](#)]
33. Zuo, L. Effective and robust vibration control using series multiple tuned-mass dampers. *J. Vib. Acoust.* **2009**, *131*, 031003. [[CrossRef](#)]
34. Asami, T. Optimal design of double-mass dynamic vibration absorbers arranged in series or in parallel. *J. Vib. Acoust.* **2017**, *139*, 011015. [[CrossRef](#)]
35. Asami, T.; Mizukawa, Y.; Ise, T. Optimal design of double-mass dynamic vibration absorbers minimizing the mobility transfer function. *J. Vib. Acoust.* **2018**, *140*, 061012. [[CrossRef](#)]
36. Berardengo, M.; Høgsberg, J.; Manzoni, S.; Vanali, M.; Brandt, A.; Godi, T. LRLC-shunted piezoelectric vibration absorber. *J. Sound Vib.* **2020**, *474*, 115268. [[CrossRef](#)]
37. Du, D.; Gu, X.; Chu, D.; Hua, H. Performance and parametric study of infinite-multiple TMDs for structures under ground acceleration by H_∞ optimization. *J. Sound Vib.* **2007**, *305*, 843–853. [[CrossRef](#)]
38. Li, H.-N.; Ni, X.-L. Optimization of non-uniformly distributed multiple tuned mass damper. *J. Sound Vib.* **2007**, *308*, 80–97. [[CrossRef](#)]
39. Li, H.-N.; Liu, M.-M.; Fu, X. An innovative re-centering SMA-lead damper and its application to steel frame structures. *Smart Mater. Struct.* **2018**, *27*, 075029. [[CrossRef](#)]
40. Li, K.; Darby, A.P. A buffered impact damper for multi-degree-of-freedom structural control. *Earthq. Eng. Struct. Dyn.* **2008**, *37*, 1491–1510. [[CrossRef](#)]
41. Jiang, X.; McFarland, D.M.; Bergman, L.A.; Vakakis, A.F. Steady state passive nonlinear energy pumping in coupled oscillators: Theoretical and experimental results. *Nonlinear Dyn.* **2003**, *33*, 87–102. [[CrossRef](#)]
42. Masri, S. Theory of the dynamic vibration neutralizer with motion-limiting stops. *J. Appl. Mech.* **1972**, *39*, 563–568. [[CrossRef](#)]

43. Masri, S.F.; Caffrey, J.P. Response of Pounding Dynamic Vibration Neutralizer Under Harmonic and Random Excitation. *J. Appl. Mech.* **2019**, *86*, 021003. [[CrossRef](#)]
44. Zhang, P.; Li, L.; Patil, D.; Singla, M.; Li, H.; Mo, Y.; Song, G. Parametric study of pounding tuned mass damper for subsea jumpers. *Smart Mater. Struct.* **2015**, *25*, 015028. [[CrossRef](#)]
45. Zhang, P.; Ren, L.; Li, H.; Jia, Z.; Jiang, T. Control of wind-induced vibration of transmission tower-line system by using a spring pendulum. *Math. Probl. Eng.* **2015**. [[CrossRef](#)]
46. Carpineto, N.; Lacarbonara, W.; Vestroni, F. Hysteretic tuned mass dampers for structural vibration mitigation. *J. Sound Vib.* **2014**, *333*, 1302–1318. [[CrossRef](#)]
47. Li, K.; Darby, A. An experimental investigation into the use of a buffered impact damper. *J. Sound Vib.* **2006**, *291*, 844–860. [[CrossRef](#)]
48. Li, K.; Darby, A. Experiments on the effect of an impact damper on a multiple-degree-of-freedom system. *J. Vib. Control* **2006**, *12*, 445–464. [[CrossRef](#)]
49. Li, H.; Zhang, P.; Song, G.; Patil, D.; Mo, Y. Robustness study of the pounding tuned mass damper for vibration control of subsea jumpers. *Smart Mater. Struct.* **2015**, *24*, 095001. [[CrossRef](#)]
50. Zhang, P.; Song, G.; Li, H.-N.; Lin, Y.-X. Seismic control of power transmission tower using pounding TMD. *J. Eng. Mech.* **2012**, *139*, 1395–1406. [[CrossRef](#)]
51. Lin, W.; Wang, Q.; Li, J.; Chen, S.; Qi, A. Shaking table test of pounding tuned mass damper (PTMD) on a frame structure under earthquake excitation. *Comput. Concr.* **2017**, *20*, 545–553.
52. Zhao, N.; Lu, C.; Chen, M.; Luo, N.; Liu, C. Parametric Study of Pounding Tuned Mass Damper Based on Experiment of Vibration Control of a Traffic Signal Structure. *J. Aerosp. Eng.* **2018**, *31*, 04018108. [[CrossRef](#)]
53. Yin, X.; Song, G.; Liu, Y. Vibration suppression of wind/traffic/bridge coupled system using multiple pounding tuned mass dampers (MPTMD). *Sensors* **2019**, *19*, 1133. [[CrossRef](#)]
54. Yin, X.; Liu, Y.; Song, G.; Mo, Y. Suppression of bridge vibration induced by moving vehicles using pounding tuned mass dampers. *J. Bridge Eng.* **2018**, *23*, 04018047. [[CrossRef](#)]
55. Wang, W.; Wang, X.; Hua, X.; Song, G.; Chen, Z. Vibration control of vortex-induced vibrations of a bridge deck by a single-side pounding tuned mass damper. *Eng. Struct.* **2018**, *173*, 61–75. [[CrossRef](#)]
56. Song, G.; Zhang, P.; Li, L.; Singla, M.; Patil, D.; Li, H.; Mo, Y. Vibration control of a pipeline structure using pounding tuned mass damper. *J. Eng. Mech.* **2016**, *142*, 04016031. [[CrossRef](#)]
57. Jiang, J.; Zhang, P.; Patil, D.; Li, H.N.; Song, G. Experimental studies on the effectiveness and robustness of a pounding tuned mass damper for vibration suppression of a submerged cylindrical pipe. *Struct. Control Health Monit.* **2017**, *24*, e2027. [[CrossRef](#)]
58. Tan, J.; Ho, M.; Chun, S.; Zhang, P.; Jiang, J. Experimental Study on Vibration Control of Suspended Piping System by Single-Sided Pounding Tuned Mass Damper. *Appl. Sci.* **2019**, *9*, 285. [[CrossRef](#)]
59. Li, S.; Sun, L.; Kong, F. Vibration Control Performance Analysis and Shake-Table Test of a Pounding Tuned Rotary Mass Damper under the Earthquake. *Shock. Vib.* **2019**, *2019*, 1–14. [[CrossRef](#)]
60. Liu, M.; Yang, W.; Chen, W.; Li, H. Experimental investigation on multi-mode vortex-induced vibration control of stay cable installed with pounding tuned mass dampers. *Smart Struct. Syst.* **2019**, *23*, 579–587.
61. Tan, J.; Jiang, J.; Liu, M.; Feng, Q.; Zhang, P.; Ho, S.C.M. Implementation of Shape Memory Alloy Sponge as Energy Dissipating Material on Pounding Tuned Mass Damper: An Experimental Investigation. *Appl. Sci.* **2019**, *9*, 1079. [[CrossRef](#)]
62. Wang, W.; Hua, X.; Chen, Z.; Wang, X.; Song, G. Modeling, simulation, and validation of a pendulum-pounding tuned mass damper for vibration control. *Struct. Control Health Monit.* **2019**, *26*, e2326. [[CrossRef](#)]
63. Collette, F.S. A combined tuned absorber and pendulum impact damper under random excitation. *J. Sound Vib.* **1998**, *216*, 199–213. [[CrossRef](#)]
64. Wang, D. Analysis of vibration energy dissipation with vibro-impact absorber. *J. Mech. Eng.* **2014**, *50*, 87–92. [[CrossRef](#)]
65. Lin, W.; Lin, Y.; Song, G.; Li, J. Multiple Pounding Tuned Mass Damper (MPTMD) control on benchmark tower subjected to earthquake excitations. *Earthq. Struct.* **2016**, *11*, 1123–1141. [[CrossRef](#)]
66. Lin, W.; Song, G.; Chen, S. PTMD Control on a Benchmark TV Tower under Earthquake and Wind Load Excitations. *Appl. Sci.* **2017**, *7*, 425. [[CrossRef](#)]
67. Fu, X.; Li, H.N.; Li, J.X.; Zhang, P. A pounding spacer damper and its application on transmission line subjected to fluctuating wind load. *Struct. Control Health Monit.* **2017**, *24*, e1950. [[CrossRef](#)]
68. Tian, L.; Rong, K.; Bi, K.; Zhang, P. A Bidirectional Pounding Tuned Mass Damper and its Application to Transmission Tower-Line Systems under Seismic Excitations. *Int. J. Struct. Stab. Dyn.* **2019**. [[CrossRef](#)]
69. Wang, W.; Hua, X.; Wang, X.; Chen, Z.; Song, G. Numerical modeling and experimental study on a novel pounding tuned mass damper. *J. Vib. Control* **2018**, *24*, 4023–4036. [[CrossRef](#)]
70. Ghasemi, M.R.; Shabakhty, N.; Enferadi, M.H. Vibration control of offshore jacket platforms through shape memory alloy pounding tuned mass damper (SMA-PTMD). *Ocean Eng.* **2019**, *191*, 106348. [[CrossRef](#)]
71. Yang, Z.; Xia, Q.; Liu, S. The spring pendulum under different controlled parameters. *Coll. Phys.* **2011**, *5*, 23–26+42.
72. Wang, J.; Liu, H.; Yuan, D.; Xu, Z. An improved state space model for parts of nonlinear oscillation systems and its numerical method. *Chin. J. Appl. Mech.* **2002**, *112*, 116–167. [[CrossRef](#)]

-
73. Chandra, M. Spring Pendulum: A Nonlinear Paradigm. 2018. Available online: <https://ssrn.com/abstract=3306010> or <http://dx.doi.org/10.2139/ssrn.3306010> (accessed on 1 March 2019).
 74. DL/T. *Technical Code for the Design of Tower and Pole Structures of Overhead Transmission Line*; China Planning Press: Beijing, China, 2012.
 75. Saidi, I.; Gad, E.; Wilson, J.L.; Haritos, N. Development of passive viscoelastic damper to attenuate excessive floor vibrations. *Eng. Struct.* **2011**, *33*, 3317–3328. [[CrossRef](#)]